Climate Variability & Models

Impact of Increasing Atmospheric CO_2 Concentration on Global Temperature & Precipitation

Using the Planet Simulator

Robert Wright

20th February 2023

1. Introduction

Rising global mean temperature due to an increase of greenhouse gases is one of the major challenges that humankind faces. Already, the consequent change in precipitation patterns has led to severe disasters, such as flooding, heavy rain and droughts. Hence, it is of interest to investigate the development of temperature and precipitation under an increase of CO_2, the primary greenhouse gas emitted through human activities [IPC14]. On top, both parameters can be combined into an aridity index, (hopefully) reasonably pinpointing regions which are going to be highly affected by an increase in atmospheric CO_2 concentration.

Climate models are vital to simulate and resolve future climate change scenarios. In order to select appropriate CO_2 concentrations for the simulations, we take *Shared Socioeco-*

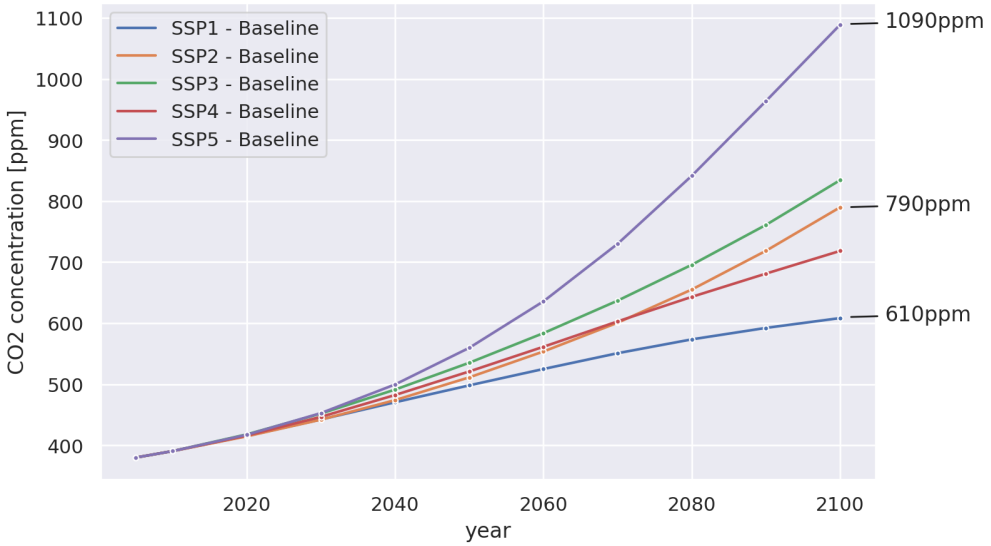

Figure 1: **Projected CO_2 concentrations of SSPs.** The annotated values are the expected CO_2 concentrations by 2100 of the three chosen pathways and used as parameters in this study.

nomic Pathways (SSPs) defined by the Intergovernmental Panel on Climate Change (IPCC) into account. The SSPs are climate scenarios based on varying political actions (from sustainability to fossil-fueled development) and can be used to derive global greenhouse gas emissions [Ria+17]. Figure 1 displays the projected increase of atmospheric CO_2 concentration for different (baseline) SSPs.

2. Data

The Planet Simulator (PlaSim) is a climate model of intermediate complexity that was developed by the university of Hamburg [Fra+05]. It features an atmospheric global circulation model, a simple mixed ocean layer model, dynamic sea ice, vegetation and topography, however, PlaSim does not include a stratosphere. The model can be adjusted by altering various parameters, in this study, the atmospheric CO_2 concentration is set to a constant value (see fig. 1; reference CO_2 concentration is 360 ppm). Lunkeit et al. [Lun+11] provide further information about running simulations with PlaSim.

The simulations are computed with the default 'T21' resolution, i.e., 32×64 cells on a latitude-longitude grid. The starting year is set to 2000 and simulations run for 30 years – it is assumed that during the last ten years an equilibrium state has been reached, thus, only data from this time interval is considered in the following. The daily temperature at 2 m and precipitation data is preprocessed using *Climate Data Operators* [Sch22], eventually leading to two datasets for each variable:

1. **No temporal dimension**. When calculating annual means (sums), daily values of each simulation year are averaged (aggregated). This results in a single value per year, which is combined to get a climatology.

2. **Including temporal dimension**. If the time domain is of interest, we calculate 5-day means/sums, then, we compute a multi-year average to obtain a single year with 73 time steps.

Depending on whether the spatial domain is kept or not, the computations listed above are either performed on individual grid cells or on globally averaged/aggregated values. Whenever anomalies are shown, the reference simulation is subtracted from the SSP simulation, and anomalies smaller than 5 % of the absolute maximum value are masked. Please refer to appendix A for further details on data processing.

3. Aridity Index

Aridity indices are a measure of water availability, which in turn is vital for plants, animals and humans. Generally speaking, the indices quantify the uptake and loss of water in the ecosystem of a region. To date, more than 50 aridity indices have been proposed [Qua+13]. Often, evaporation is approximated using temperature, however, some indices also include evapotranspiration (ET), which combines *transpiration* and soil *evapo*ration to describe how water moves from the earth's surface to the atmosphere [Sta05]. Here, since computing ET is a complex process, we chose to evaluate the approximation by Martonne

[Mar26], who defined the aridity index as

$$AI_{dM} = \frac{P_A}{T_A + 10}, \tag{1}$$

where P_A is the annual precipitation sum in mm and T_A is the mean annual temperature in °C. Following an approach of Grieser et al. [Gri+06], we circumvent the pole of eq. (1) at $-10\,°\mathrm{C}$ by adjusting the aridity index to

$$AI_{dM} = \begin{cases} 100, & \text{if } T_A < -9.9\,°\mathrm{C} \\ AI_{dM}, & \text{otherwise.} \end{cases} \tag{2}$$

Hence, AI_{dM} is a dimensionless, solely positive quantity. The higher (lower) the aridity index, the higher (lower) is precipitation compared to evaporation, indicating humid (arid) climate. The adjustment of eq. (2) is useful for calculating the aridity index on a global scale, however, one may argue that the concept of aridity is not applicable in cold regions anyway.

4. Results & Discussion

This section starts with an overview of global averages of temperature and precipitation for each PlaSim run, then, shifting the focus towards changes in precipitation patterns with increasing CO_2 concentration, and ultimately quantifying the impact and consequences of those changes by spatially visualizing moisture regimes of the different climate scenarios.

4.1. Global Warming

The increase in global mean temperature amongst the different PlaSim runs is displayed in fig. 2. A linear fit reveals a global warming of $(0.98 \pm 0.11) \times 10^{-2}\,\mathrm{K\,ppm^{-1}}$, however, it is important to note that we are only comparing equilibrium states of constant CO_2

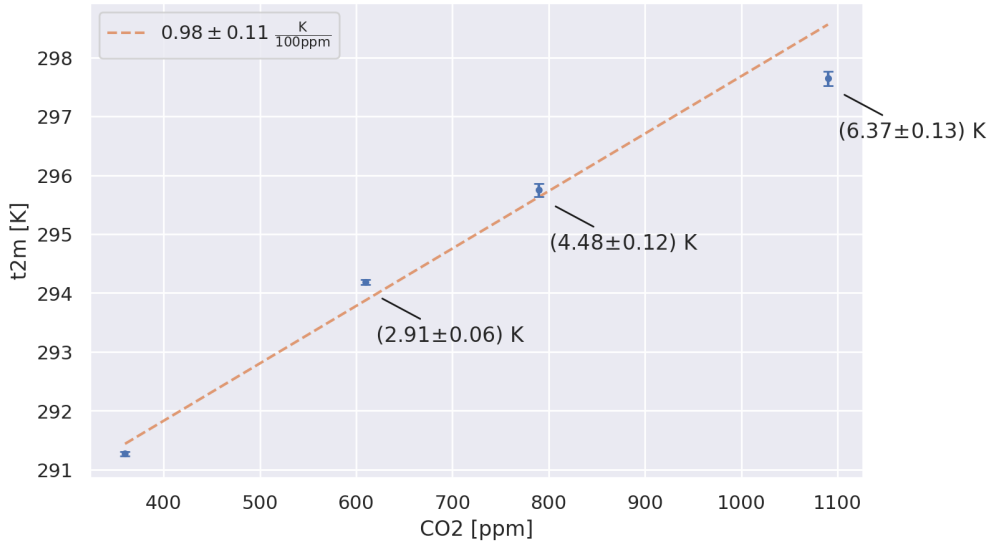

Figure 2: **Global mean temperature (increase) for different CO_2 concentrations**. The increase in temperature of the respective SSP simulation compared to the reference is annotated. The dashed line is a linear fit taking into account the uncertainties of predicted temperature values.

concentration. On top, uncertainty is large in literature, e.g., Richardson et al. [Ric+16] predict a global CO_2 concentration of 429 ppm to 1069 ppm (90 % confident interval) for a global warming of 2 °C, thus, agreeing with our predictions, but effectively covering the entire CO_2 concentration range of the simulations.

Experiment name	CO_2 concentration [ppm]	Temperature increase [K]	Precipitation sum [m/yr]
Reference	360	-	1207.6 ± 2.3
SSP1	610	2.91 ± 0.06	1287.8 ± 2.7
SSP3	790	4.48 ± 0.12	1333.4 ± 2.3
SSP5	1090	6.37 ± 0.13	1394 ± 4

Table 1: Simulation parameter and global mean of study variables.

Including the globally-averaged annual precipitation sum, we can summarize the findings (omitting the time and spatial domain) in table 1. Globally speaking, mean temperature and precipitation sum are both increasing with higher atmospheric CO_2 concentration.

4.2. Precipitation Anomalies

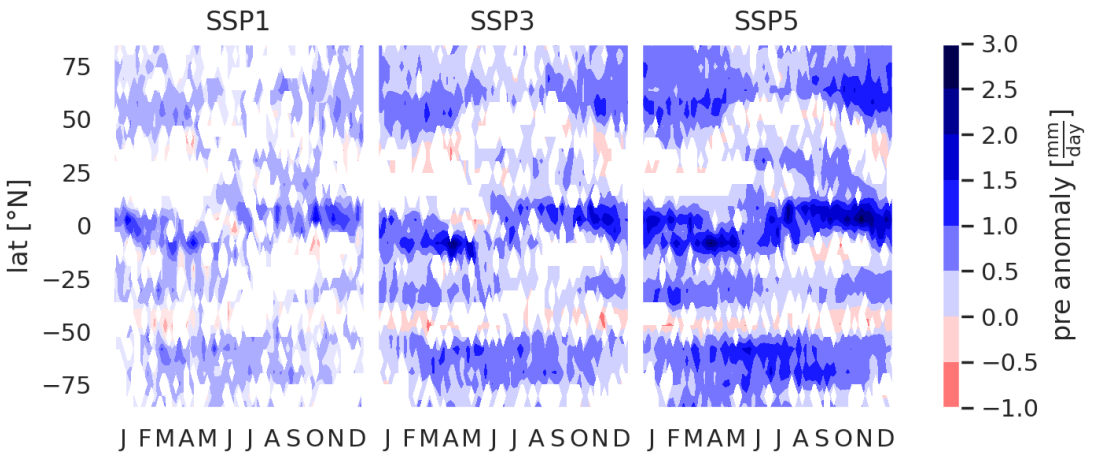

Figure 3: **Zonal mean of precipitation anomaly** derived from dataset with time domain. Labels on x-axis correspond to the first letter of the month. Absolute anomalies smaller than $0.14\,\mathrm{mm\,d^{-1}}$ are excluded.

The zonal mean anomalies in fig. 3 reveal that the change in precipitation pattern is most likely caused by an intensification of the global atmospheric circulation. Consequently, the strongest increase in daily precipitation can be seen at the intertropical convergence zone (ITCZ) close to the equator (rising air), while in the higher latitudes at around 30 °N and −30 °N, where the Hadley and Ferell cell converge, only small or even negative anomalies are detected (sinking air). A seasonal shift can be observed in the northern hemisphere, however, in the southern hemisphere the bands of small and large anomalies remain relatively constant throughout the year.

Accordingly, fig. 4 also illustrates the zonal bands of large and small anomalies corresponding to the global atmospheric circulation patterns. However, we can clearly see regional differences and spots of more extreme precipitation anomalies. In particular, the area around the Indian Ocean, south-east Asia and Oceania shows strong changes in precipitation. On top, the overall pattern of precipitation anomalies stays similar for increasing CO_2 concentration, while the magnitude and significance of the signal increases.

The reference (fig. 6) in appendix B displays strong negative anomalies, which are not present in our analysis – neither are the positive anomalies in North Africa and the Arctic

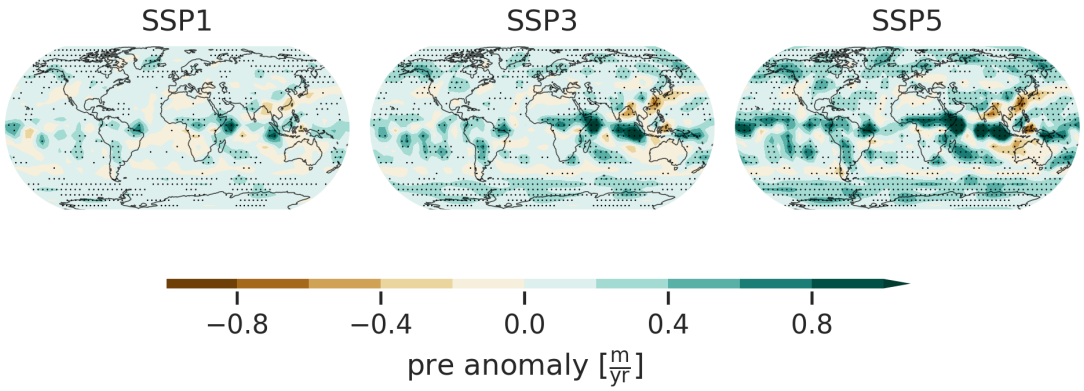

Figure 4: **Global precipitation anomalies** derived from dataset with no time domain. Significance is determined by using Welch's t-test (two-sided) for the null hypothesis (H_0) that two independent population means with different standard deviations have identical values. The alternative hypothesis H_1 is defined as population means being unequal and is accepted if p-value is below threshold of 1 %. Rejection of H_0 (i.e., unequal population means) is indicated by black dots. Absolute anomalies smaller than 0.1 m yr^{-1} are excluded.

region. However, Allan et al. [All+21] note that high anomalies in dry regions do not necessarily imply large absolute changes.

4.3. Moisture Regimes

Index range	Classification
$AI_{dM} \leq 5$	arid
$5 < AI_{dM} < 20$	moderate
$20 \leq AI_{dM} \leq 30$	humid
$AI_{dM} > 30$	perhumid

Table 2: Classification of aridity index intervals into discrete moisture regimes according to Quan et al. [Qua+13].

The aridity index can be translated into moisture regimes (see table 2). By combining precipitation and temperature (the latter as a proxy for evaporation), we can identify major climate regions in fig. 5. Deserts, such as the Sahara, are labelled as *dry*, whereas

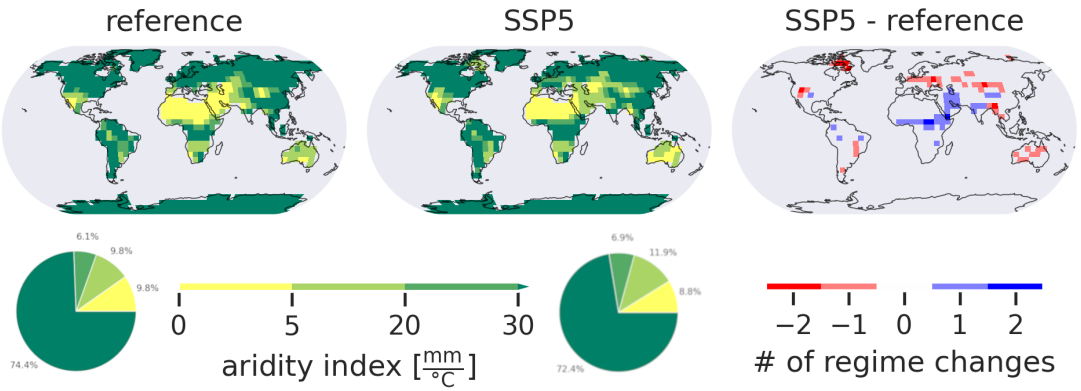

Figure 5: **Moisture regimes (and change) based on aridity index**. Oceans are masked. *Left*: Map of discrete regimes for reference simulation and highest CO_2 concentration. Colorbar levels correspond to classifications. The number of grid cells per regime (and total proportion) is shown in the pie chart below the respective map. *Right:* Number of 'steps' in different moisture regime classifications for individual grid cells, e.g., −2 might imply a change from *perhumid* in reference to *moderate* in SSP5 simulation.

regions with rainforest are detected as *perhumid*. The total number of regime labels stays relatively constant, for the high CO_2 concentration we observe a small decrease in *dry* and *perhumid* classifications and an increase in *moderate* labellings. Additionally, a qualitative comparison with fig. 7 in appendix B yields a reasonable similarity, hence, improving the reliability of our results.

Beyond, a shift in moisture regime classification for a particular region is most likely going to trigger devastating environmental changes affecting entire ecosystems and populations. Comparing reference and SSP5 simulation in fig. 5 (*left*) illustrates that in future scenarios high latitudes tend to be associated with drier regimes and regions around the equator (especially at the edge of relatively dry areas in Central Africa) are turning into humid regimes. It has to be noted though that many grid cells do not show a different classification and (strong) signals are regionally bound.

5. Conclusion

This analysis quantified the increase in global mean temperature depending on atmospheric CO_2 concentration using PlaSim data. Not only temperature, but also annual precipitation sum is going to increase in high CO_2 concentration scenarios. This change is not equally distributed in space, but closely follows the global atmospheric circulation pattern. By implementing a moisture regime classification, we identified regions experiencing severe alternations in water availability, which is probably most notable for future generations.

References

[All+21] R. P. Allan et al. 'IPCC, 2021: Summary for Policymakers'. In: *Climate Change 2021: The Physical Science Basis. Contribution of Working Group I to the Sixth Assessment Report of the Intergovernmental Panel on Climate Change*. Ed. by V. Masson-Delmotte et al. Cambridge University Press, Aug. 2021, pp. 3–32. DOI: 10.1017/9781009157896.001.

[Fra+05] K. Fraedrich et al. 'The Planet Simulator: Towards a user friendly model'. In: *Meteorologische Zeitschrift* 14.3 (July 2005), pp. 299–304. DOI: 10.1127/0941-2948/2005/0043.

[Gri+06] J. Grieser et al. *New gridded maps of Koeppen's climate classification*. Jan. 2006.

[IPC14] IPCC. 'Summary for Policymakers'. In: *Climate Change 2013 – The Physical Science Basis: Working Group I Contribution to the Fifth Assessment Report of the Intergovernmental Panel on Climate Change*. Cambridge University Press, 2014, pp. 1–30. DOI: 10.1017/CBO9781107415324.004.

[Lun+11] F. Lunkeit et al. *Planet Simulator Reference Manual Version 16*. Hamburg, Germany, 2011.

[Mar26] E. de Martonne. 'Aréisme et indice d'aridité'. In: *Comptes Rendus Académie des Sciences* 181 (1926), pp. 1395–1398.

[Qua+13] C. Quan et al. 'Validation of temperature–precipitation based aridity index: Paleoclimatic implications'. In: *Palaeogeography, Palaeoclimatology, Palaeoecology* 386 (Sept. 2013), pp. 86–95. DOI: 10.1016/j.palaeo.2013.05.008.

[Ria+17] K. Riahi et al. 'The Shared Socioeconomic Pathways and their energy, land use, and greenhouse gas emissions implications: An overview'. In: *Global Environmental Change* 42 (Jan. 2017), pp. 153–168. DOI: 10.1016/j.gloenvcha.2016.05.009.

[Ric+16] M. Richardson et al. 'Reconciled climate response estimates from climate models and the energy budget of Earth'. In: *Nature Climate Change* 6.10 (June 2016), pp. 931–935. DOI: 10.1038/nclimate3066.

[Sch22] U. Schulzweida. *CDO User Guide*. Version 2.1.0. Oct. 2022. DOI: 10.5281/zenodo.7112925.

[Sta05] G. Stanhill. 'Evapotranspiration'. In: *Encyclopedia of Soils in the Environment*. Elsevier, 2005, pp. 502–506. DOI: 10.1016/b0-12-348530-4/00359-3.

A. Code Availability

The python code for this (environmental) data analysis can be found in an online repository[1]; bash scripts for preprocessing the climate model output are inside the `data`-directory.

B. Reference Figures

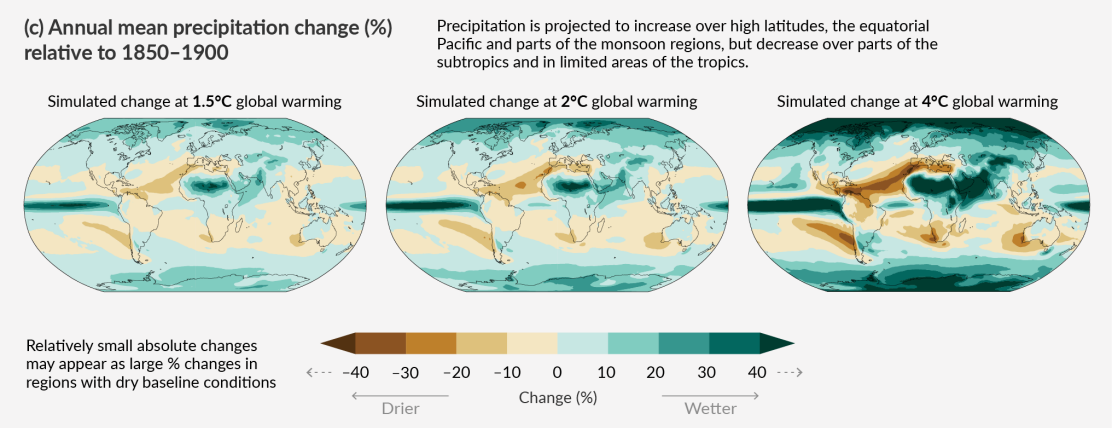

Figure 6: **Simulated changes in mean precipitation** as illustrated by the latest IPCC report [All+21].

[1] https://github.com/vegan-schnitzel/moisture-regimes

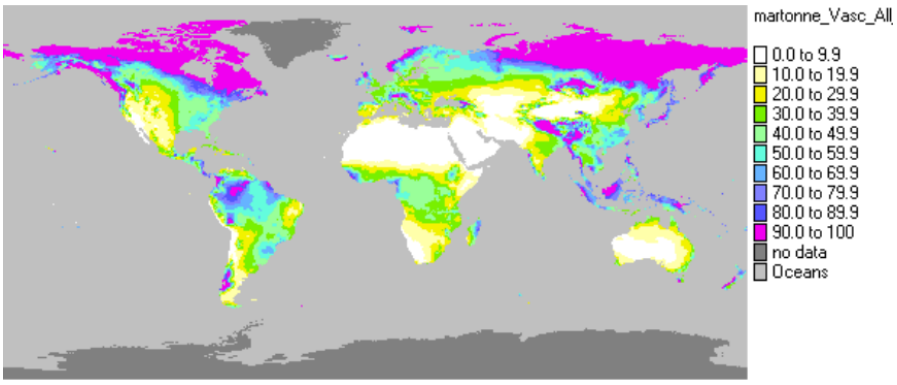

Figure 7: **Global map of aridity index** (AI_{dM}) for the 50 yr period from 1951 to 2000 based on reanalysis data by Grieser et al. [Gri+06].